© 2019. Published by The Company of Biologists Ltd | Journal of Cell Science (2019) 132, jcs237750. doi:10.1242/jcs.237750

CORRECTION

Correction: Spindle checkpoint silencing at kinetochores with submaximal microtubule occupancy (doi:10.1242/jcs.231589)

Banafsheh Etemad, Abel Vertesy, Timo E. F. Kuijt, Carlos Sacristan, Alexander van Oudenaarden and Geert J. P. L. Kops

There were errors in *J. Cell Sci*. (2019) **132**, jcs231589 (doi:10.1242/jcs.231589).

Labels for Spindly, MAD2 and ZW10 were incorrect in Fig. 2C. In Figs S1 and S2, a biological replicate of pMELT that had technical issues was inadvertently used. Replicate e2 has been replaced for pMELT in Fig. S1D,E and analysis of the pMELT samples in Fig. S3C,D,F has been corrected. The corrected main and supplementary figures are shown here, along with the original versions for reference.

The online and PDF versions of the article and the supplementary material have been updated. The authors apologise to readers for these errors, which do not impact the conclusions of the paper.

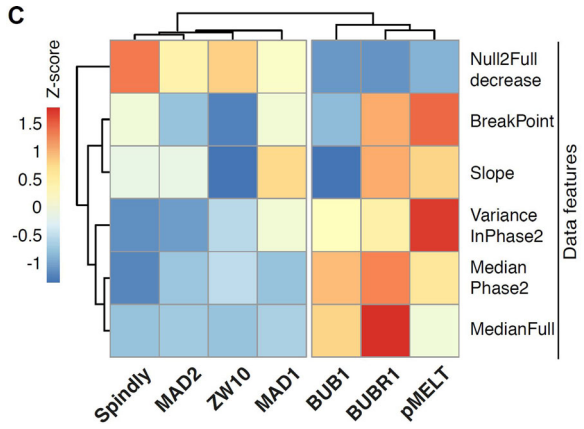

Fig. 2C (corrected panel). Microtubule attachments evoke two distinct SAC protein responses. (C) Hierarchical cluster analysis of Z-score normalized features extracted from data in Fig. 1B-H as depicted in B.

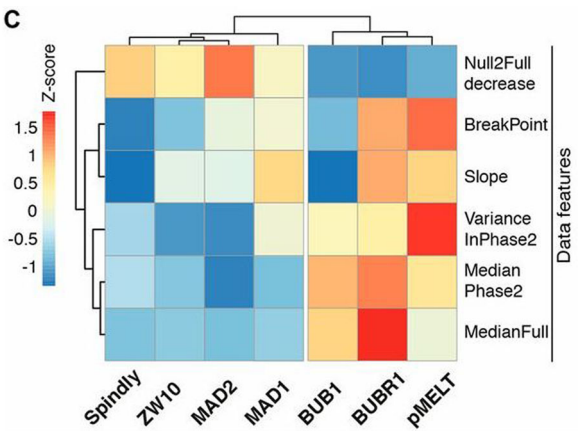

Fig. 2C (original panel). Microtubule attachments evoke two distinct SAC protein responses. (C) Hierarchical cluster analysis of Z-score normalized features extracted from data in Fig. 1B-H as depicted in B.

Journal of Cell Science (2019) 132, jcs237750. doi:10.1242/jcs.237750

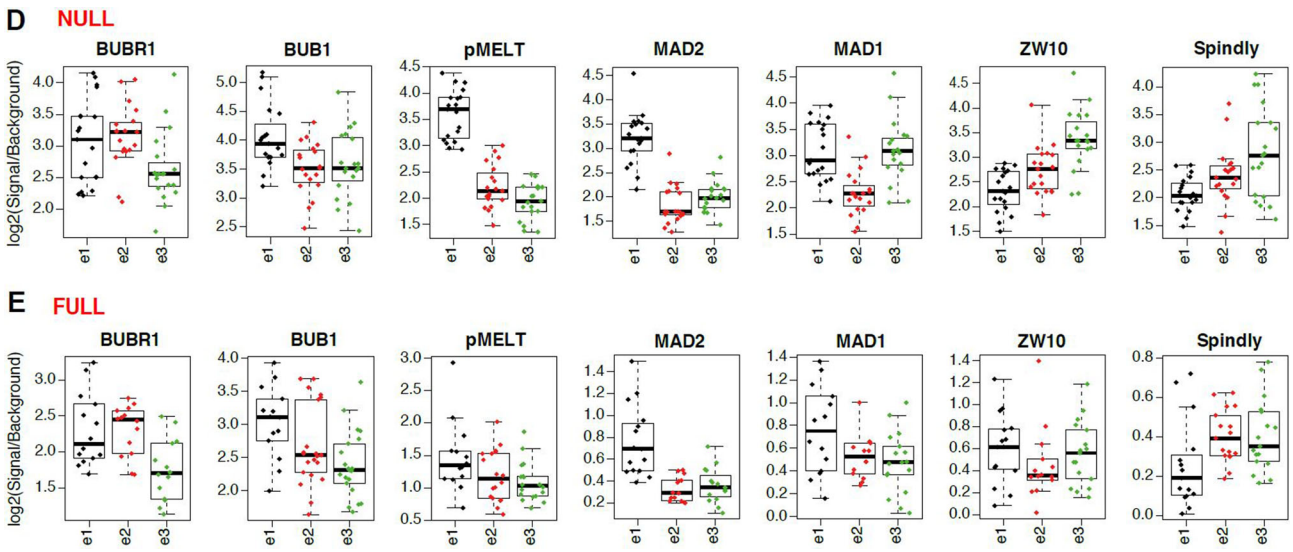

Fig. S1D,E (corrected panels). Single kinetochore measurements reveal differences between SAC protein localization independent of signal-to-noise ratios. (D,E) Signal-to-noise ratios of SAC proteins measured on kinetochores of unattached (D, 'NULL') and fully microtubule-occupied kinetochores (E, 'FULL'). Each biological replicate is plotted separately and represented by 'e1', 'e2', and 'e3'. All proteins and experiments in NULL condition (D) show similar signal-to-noise ratios, suggesting that variability in values measured in this condition is equally affected by noise across all experiments. In the FULL condition (E) signal-to-noise ratio is much better in proteins with kinetochore retention and high variation (BUB1, BUBR1, and pMELT), strongly supporting that the observed behavior (shown in Figure 1B-H) is not due to skewed signal intensities.

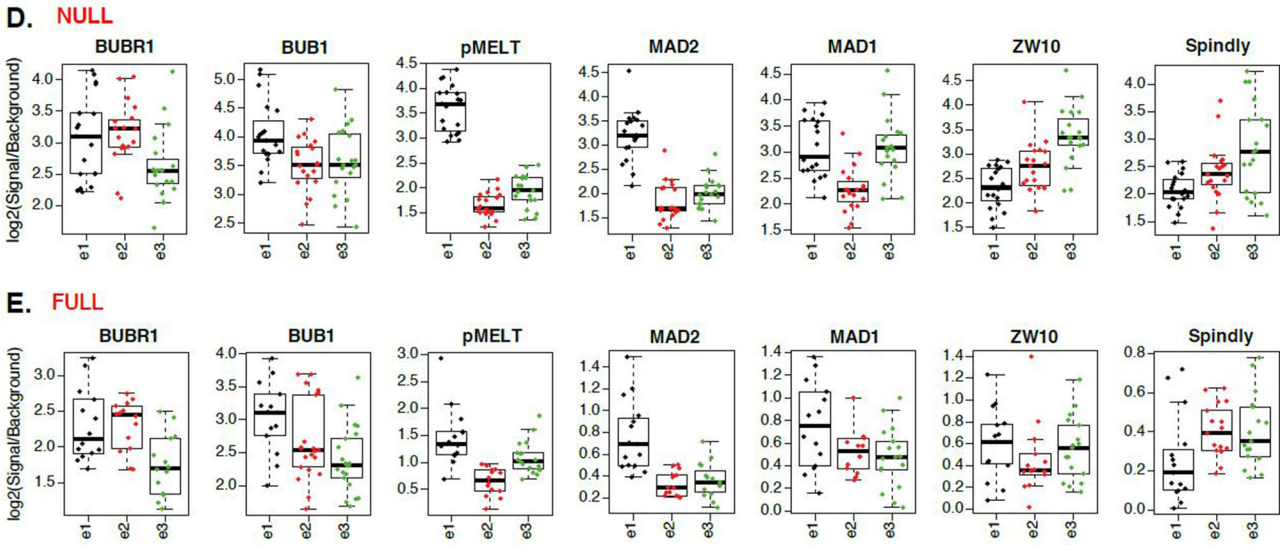

Fig. S1D,E (original panels). Single kinetochore measurements reveal differences between SAC protein localization independent of signal-to-noise ratios. (D,E) Signal-to-noise ratios of SAC proteins measured on kinetochores of unattached (D, 'NULL') and fully microtubule-occupied kinetochores (E, 'FULL'). Each biological replicate is plotted separately and represented by 'e1', 'e2', and 'e3'. All proteins and experiments in NULL condition (D) show similar signal-to-noise ratios, suggesting that variability in values measured in this condition is equally affected by noise across all experiments. In the FULL condition (E) signal-to-noise ratio is much better in proteins with kinetochore retention and high variation (BUB1, BUBR1, and pMELT), strongly supporting that the observed behavior (shown in Figure 1B-H) is not due to skewed signal intensities.

Journal of Cell Science (2019) 132, jcs237750. doi:10.1242/jcs.237750

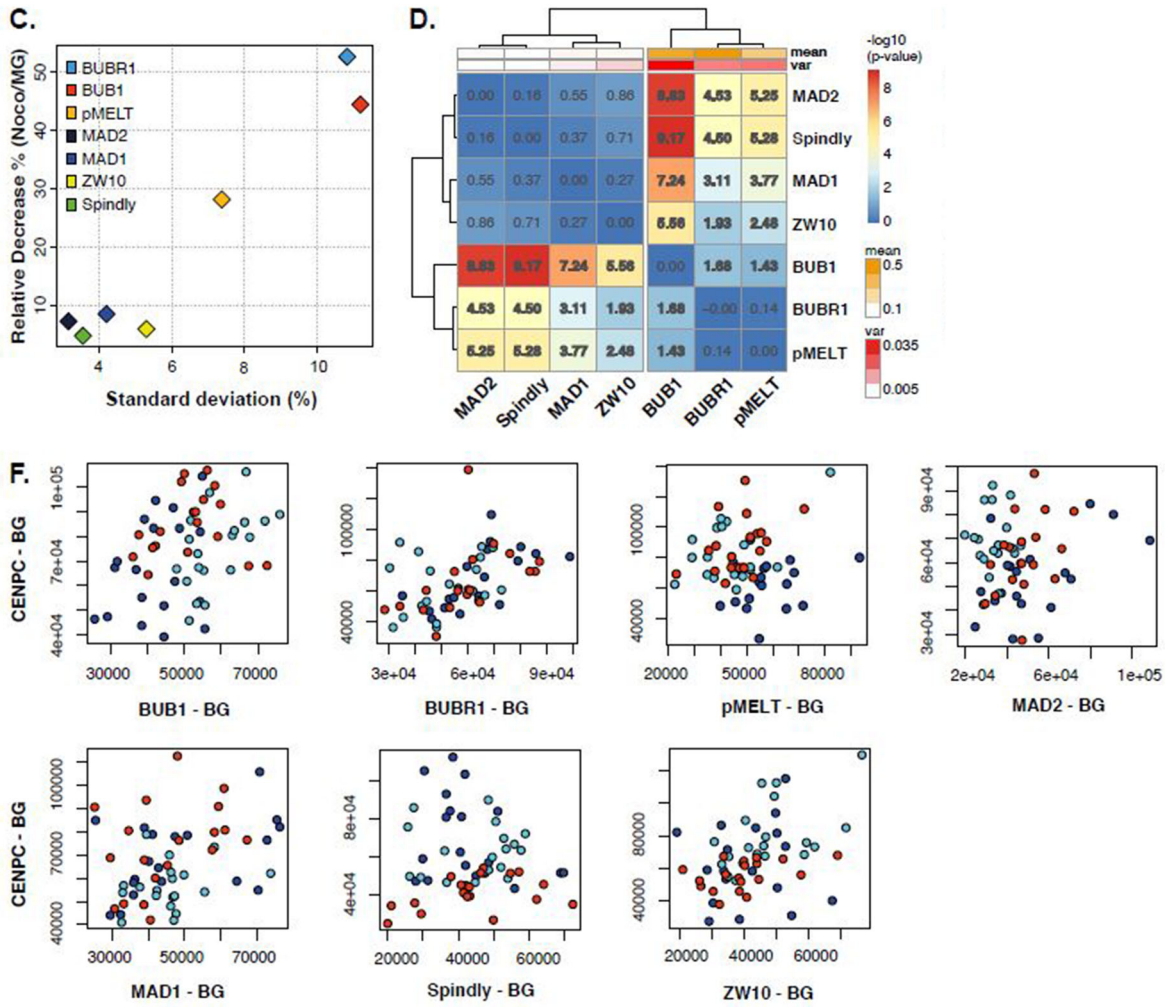

Fig. S3C,D,F (corrected panels). High variability of protein levels on unattached kinetochores is independent of CENP-C levels, the kinetochore size, antibody penetration or differences between replicates. (C) Plot depicting correlation between the relative protein decrease from NULL to FULL conditions and the standard deviation measured at FULL attachment (data shown in insets of Figure 1 B-H). (D) To test how similar the variability of the FULL datasets (insets Figure 1B-H) between different SAC proteins are, we applied pairwise Levene's test. Figure shows clustering heat map of P-values from these tests. –log10(p-values) are displayed. Significant differences are in bold. Top bars represent variance (red) and average levels (orange) of each protein. (F) Staining efficiency is similar in the biological replicates of experiments shown in Figure 1. Graphs show background (BG)-corrected levels of SAC proteins at unattached kinetochores, plotted against corresponding BG-corrected CENP-C levels. Different colors depict individual experiments.

Journal of Cell Science (2019) 132, jcs237750. doi:10.1242/jcs.237750

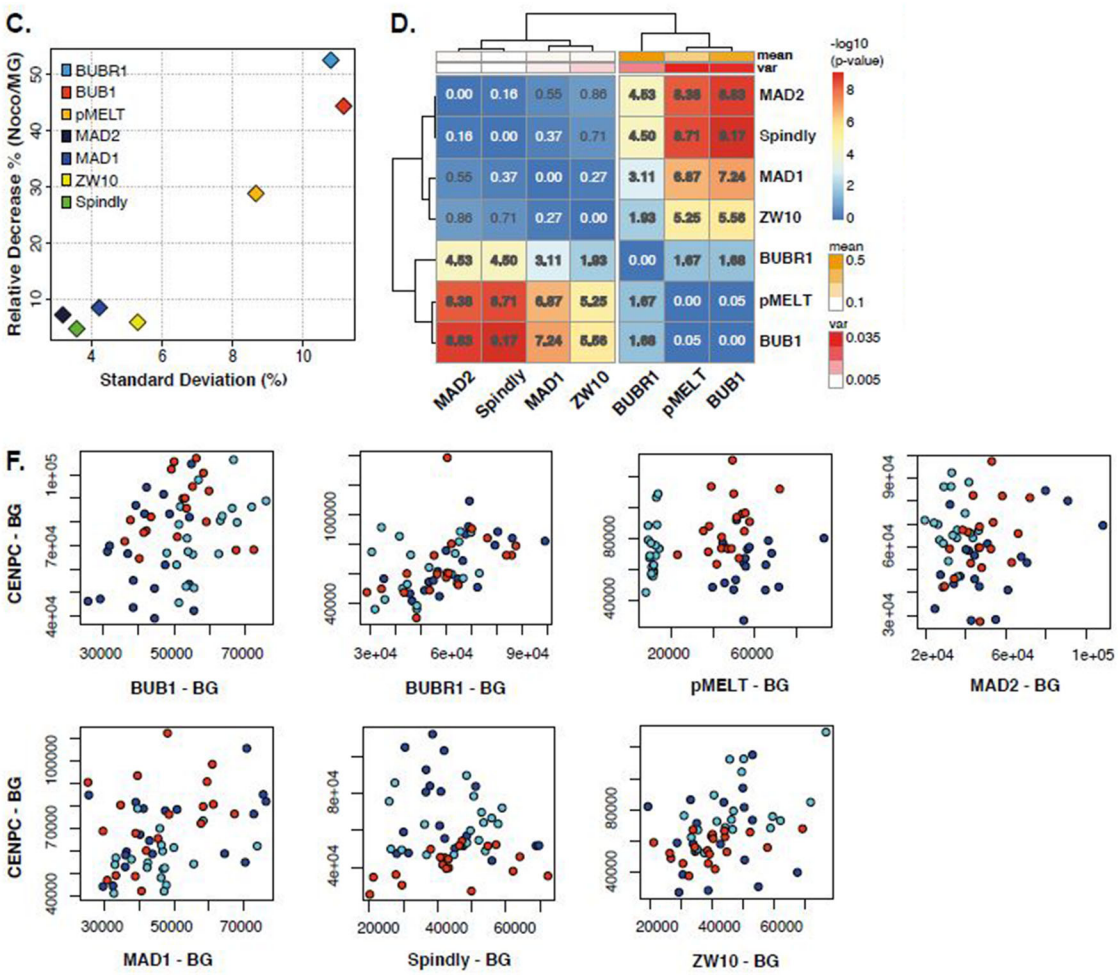

Fig. S3C,D,F (original panels). High variability of protein levels on unattached kinetochores is independent of CENP-C levels, the kinetochore size, antibody penetration or differences between replicates. (C) Plot depicting correlation between the relative protein decrease from NULL to FULL conditions and the standard deviation measured at FULL attachment (data shown in insets of Figure 1 B-H). (D) To test how similar the variability of the FULL datasets (insets Figure 1B-H) between different SAC proteins are, we applied pairwise Levene's test. Figure shows clustering heat map of P-values from these tests. –log10(p-values) are displayed. Significant differences are in bold. Top bars represent variance (red) and average levels (orange) of each protein. (F) Staining efficiency is similar in the biological replicates of experiments shown in Figure 1. Graphs show background (BG)-corrected levels of SAC proteins at unattached kinetochores, plotted against corresponding BG-corrected CENP-C levels. Different colors depict individual experiments.

© 2019. Published by The Company of Biologists Ltd | Journal of Cell Science (2019) 132, jcs231589. doi:10.1242/jcs.231589

RESEARCH ARTICLE

Spindle checkpoint silencing at kinetochores with submaximal microtubule occupancy

Banafsheh Etemad, Abel Vertesy, Timo E. F. Kuijt, Carlos Sacristan, Alexander van Oudenaarden and Geert J. P. L. Kops*

ABSTRACT

The spindle assembly checkpoint (SAC) ensures proper chromosome segregation by monitoring kinetochore–microtubule interactions. SAC proteins are shed from kinetochores once stable attachments are achieved. Human kinetochores consist of hundreds of SAC protein recruitment modules and bind up to 20 microtubules, raising the question of how the SAC responds to intermediate attachment states. We show that one protein module ('RZZS-MAD1-MAD2') of the SAC is removed from kinetochores at low microtubule occupancy and remains absent at higher occupancies, while another module ('BUB1-BUBR1') is retained at substantial levels irrespective of attachment states. These behaviours reflect different silencing mechanisms: while BUB1 displacement is almost fully dependent on MPS1 inactivation, MAD1 (also known as MAD1L1) displacement is not. Artificially tuning the affinity of kinetochores for microtubules further shows that ∼50% occupancy is sufficient to shed MAD2 and silence the SAC. Kinetochores thus respond as a single unit to shut down SAC signalling at submaximal occupancy states, but retain one SAC module. This may ensure continued SAC silencing on kinetochores with fluctuating occupancy states while maintaining the ability for fast SAC re-activation.

KEY WORDS: Chromosome segregation, Kinetochore, Microtubules, Mitosis, Spindle assembly checkpoint

INTRODUCTION

Errors in chromosome segregation cause aneuploid karyotypes, which are devastating to embryonic development and are strongly associated with cancer (de Wolf and Kops, 2017; Duijf et al., 2013; Hanahan and Weinberg, 2011; Ricke and van Deursen, 2013). To ensure proper chromosome segregation, the spindle assembly checkpoint (SAC) prevents anaphase initiation until all chromosomes are stably attached to spindle microtubules. These attachments are powered by kinetochores, specialized structures assembled on centromeric chromatin (Musacchio and Desai, 2017). Microtubule binding by kinetochores is mediated predominantly by the NDC80 complex (Cheeseman et al., 2006; DeLuca and Musacchio, 2012; DeLuca et al., 2002; Tooley and Stukenberg, 2011). When unbound by microtubules, however, this complex recruits the MPS1 kinase (also known as TTK) to kinetochores (Hiruma et al., 2015; Ji et al., 2015; Liu and Winey, 2012), where it initiates a cascade of events that culminates in production of the anaphase inhibitor. The cascade involves phosphorylation of the short linear MELT sequences in the kinetochore protein KNL1 to form the binding sites for the BUB3-bound SAC proteins BUBR1 and BUB1 (Krenn et al., 2014; Overlack et al., 2015; Primorac et al., 2013; Vleugel et al., 2013; Zhang et al., 2014). MPS1 also ensures localization of the MAD1–MAD2 complex (also known as MAD1L1 and MAD2L1, respectively), at least in part by promoting BUB1–MAD1 interactions (Kim et al., 2012; London and Biggins, 2014; Silió et al., 2015). MAD1–MAD2 recruitment additionally requires the RZZ (ROD-ZW10-Zwilch) kinetochore complex but the mechanism of this has not been elucidated (Caldas et al., 2015; Matson and Stukenberg, 2014; Silió et al., 2015). Although poorly understood at the molecular level, a subset of these SAC proteins then form a multiprotein assembly with potent anaphase inhibitory activity (Chao et al., 2012; Herzog et al., 2009; Kulukian et al., 2009; Sudakin et al., 2001).

Whereas recruitment of SAC proteins to kinetochores is essential for proper SAC activation, their removal is crucial for efficient SAC silencing and timely anaphase onset (Ballister et al., 2014; Ito et al., 2012; Jelluma et al., 2010; Kuijt et al., 2014; Maldonado and Kapoor, 2011). Microtubule attachments disrupt SAC signalling from kinetochores by mediating poleward transport of SAC proteins by the dynein motor complex (a process referred to as 'stripping') (Howell et al., 2001), and by affecting the balance of SAC-regulating kinases and phosphatases (Etemad and Kops, 2016; Funabiki and Wynne, 2013; Saurin, 2018). For example, RZZ–MAD1 is a cargo of dynein via interactions with the kinetochore-specific dynactin adaptor Spindly (SPDL1) (Barisic et al., 2010; Caldas et al., 2015; Chan et al., 2009; Gassmann et al., 2008; Kops et al., 2005; Silió et al., 2015). By contrast, BUB protein removal is dependent on inhibition of local MPS1 activity and reversal of MELT phosphorylations by the PP1 phosphatase (Etemad and Kops, 2016; Hiruma et al., 2015; Ji et al., 2015; London et al., 2012; Meadows et al., 2011; Nijenhuis et al., 2014; Rosenberg et al., 2011; Zhang et al., 2014).

The subcellular architecture of kinetochores is substantially more complex than illustrated above. A single human kinetochores contains ∼240 NDC80 complexes, probably configured in a lawn-like macro-structure (Suzuki et al., 2015; Zaytsev et al., 2014). This lawn can bind up to 20 microtubules that together form a so-called kinetochore (k)-fibre (DeLuca et al., 2005; McEwen et al., 2001; Nixon et al., 2015; Wendell et al., 1993). Likewise, when unbound by microtubules, a single human kinetochore probably binds hundreds of SAC modules (Howell et al., 2004; Vleugel et al., 2015). This subcellular complexity of kinetochores raises numerous questions about the response dynamics of SAC modules to increasing amounts of bound microtubules. A current model of SAC signalling suggests that the SAC signal from kinetochores as a function of microtubule binding is not binary, but can exist in intermediate states (Collin et al., 2013). Whether SAC signalling is fully shut down only when kinetochores have acquired close to maximal microtubule occupancy is unknown (Burke and Stukenberg, 2008; Stukenberg and Burke, 2015). Two pieces of

Oncode Institute, Hubrecht Institute – KNAW and University Medical Centre Utrecht, Utrecht, 3584 CT, The Netherlands.

*Author for correspondence (g.kops@hubrecht.eu)

A.V., 0000-0001-6075-5702; G.J.P.L.K., 0000-0003-3555-5295

Received 5 March 2019; Accepted 17 May 2019

Journal of Cell Science (2019) 132, jcs231589. doi:10.1242/jcs.231589

recent evidence support a model in which submaximal occupancy is sufficient for SAC silencing: MAD1 removal is initiated before a full occupancy state is reached (Kuhn and Dumont, 2017), and reduction of microtubule occupancy at kinetochores to ∼65% using a microtubule poison cannot prevent SAC silencing (Dudka et al., 2018). It is unclear, however, what occupancy state is sufficient for SAC silencing and how the different SAC modules respond leading up to these states. Here, we address these questions by quantitative correlation imaging of SAC protein levels and microtubule occupancy at single kinetochores, and by assessing SAC activity and SAC protein levels on kinetochores with experimentally manipulated average occupancy states. Our results allow a comprehensive view of the interaction between core kinetochore proteins, SAC signalling proteins and microtubules, and how they affect mitotic exit.

RESULTS

SAC proteins respond to intermediate attachments states

Kinetochores occupied by a full complement of microtubules have decreased or diminished levels of SAC proteins. The removal dynamics of key SAC proteins in response to increased microtubule occupancy is, however, not known. To address this, we wished to simultaneously quantify the relative amounts of SAC proteins and microtubules on individual kinetochores. We developed a method that allows accurate measurements of SAC protein and tubulin signal intensities on individual kinetochores with immature k-fibres (Fig. S1A–C). MG-132 and high doses of nocodazole were used to either allow full occupancy of kinetochores ('FULL' condition) or relieve all kinetochore–microtubule attachments ('NULL' condition), respectively. To create intermediate attachments ['VAR' (variable) condition], cells were fixed in prometaphase after release from a G2/M-boundary block (see Materials and Methods for details). The resulting population of kinetochores had a mixture of attachment states (Fig. 1A), including unattached and fully attached, as evident from comparisons with simultaneous imaging of kinetochores from the NULL and FULL conditions (Fig. 1A–H). We next quantified levels of six SAC proteins (MAD1, MAD2, ZW10, Spindly, BUBR1 and BUB1) and one SAC-regulating post-translation modification [KNL1-pT180, hereafter referred to as 'pMELT' (Vleugel et al., 2015)] in all three attachment conditions on individual kinetochores, to examine SAC protein behaviour in response to microtubule attachment (Fig. 1B–H). We found that the levels of all SAC proteins were substantially reduced on kinetochores when microtubule occupancy reached ∼30% or more (relative to mean tubulin intensity in the FULL condition, which has a normalized value of 1). However, whereas most kinetochores had no or barely detectable MAD1, MAD2, ZW10 and Spindly ('RZZS-MAD1-MAD2' group) at ∼50% of mean maximum occupancy, members of the 'BUB1-BUBR1' group (pMELT, BUBR1, BUB1) remained clearly detectable and showed retention of 29–53% of the median of the levels measured on unattached kinetochores (Fig. 1B–H; insets). This is in good agreement with previous observations of SAC protein behaviour on metaphase vs prometaphase kinetochores (Bomont et al., 2005; Hoffman et al., 2001; Howell et al., 2004; Martinez-Exposito et al., 1999; Skoufias et al., 2001). Detectability of the BUB1-BUBR1 group may be due to residual MPS1 on metaphase kinetochores (Hiruma et al., 2015; Howell et al., 2004), and/or the contribution of PLK1 to BUB protein recruitment (Espeut et al., 2015; von Schubert et al., 2015). To ensure that the observed differences between the two groups did not have a technical origin, we calculated signal-to-noise ratios for the NULL and FULL conditions and found that they are similar for all proteins in our panel, supporting a biological origin of this pattern (Fig. S1D,E). In addition, the results from quantitative immuno-imaging were verified using genome-edited cell lines that express N-terminal HA-mCherry-tagged versions of MAD2 or BUB1, as representative of their groups, from their endogenous locus, excluding differences between antibodies used and/or staining efficiency as a cause for differences between SAC protein behaviour at kinetochores (Fig. S2A–F). These observations support a model in which SAC proteins respond to intermediate attachments.

Microtubule attachments evoke two types of responses on SAC proteins

Although all SAC proteins showed the expected reduction on kinetochores in cells treated with MG-132 compared to those treated with nocodazole (Howell et al., 2004) (Fig. 1B–H, whisker plots), there was substantial variation in the amount of accumulated SAC proteins on unattached kinetochores (i.e. kinetochores with very high and very low SAC protein levels) (Fig. 1B–H, insets). Variation was also observed within single cells and did not correspond to possible inter-kinetochore variation of more stable kinetochore components such as CENP-C (Fig. S3A,B) or HEC1 (also known as NDC80) (Collin et al., 2013). Inter-kinetochore variation was maintained in metaphase for the group of proteins showing substantial retention at this stage (BUB1-BUBR1 group), but not for the RZZS-MAD1-MAD2 group (Fig. 1B–H; insets Fig. S3C, *x*-axis). The cause of this variation is unclear, but one can envision an inability of phosphatases to efficiently shut down MPS1 signalling or, for example, the existence of dynamic occupancy states at metaphase to which MPS1 kinase activity is highly sensitive. Pairwise comparison of the inter-kinetochore variation of all SAC proteins in the FULL condition resulted in clustering of proteins displaying high or low variation into two distinct groups that corresponded to the RZZS-MAD1-MAD2 and BUB1-BUBR1 groups (Fig. S3D). In addition, a fraction of attached kinetochores had accumulated as much BUBR1, BUB1 and pMELT as some of their unattached counterparts (Auckland et al., 2017), which was never observed for MAD2, MAD1 and Spindly, and only to a limited extent for ZW10 (Fig. S3E). Signal-to-noise ratios in the FULL condition were similar for proteins in the BUB1-BUBR1 group, supporting a biological source for our observations (Fig. S1E). Of note, variability between kinetochores was independent of the method used for measuring local protein levels (Fig. S1A–C), of differences between biological replicates (Fig. S3F), of different antibody penetration proficiencies per cell (Fig. S3G,H), or of kinetochore size (Fig. S3I).

To further explore the different behaviour of SAC proteins in response to intermediate attachments, we performed segmented linear regression on the data presented in Fig. 1 (Fig. 2A), and hierarchical clustering of various extracted mathematical features of their response to different microtubule occupancy states (features and clustering shown in Fig. 2B,C). We chose features that are biologically relevant, such as the difference between NULL and FULL (Null2Full decrease) and the level of tubulin intensity when the minimum levels of SAC protein are reached (Breakpoint) (Fig. 2B). Interestingly, occupancy response curves separated into two clusters after hierarchical clustering: one containing the profiles of MAD1, MAD2, Spindly and ZW10 and the other containing those of BUB1, BUBR1 and pMELT (Fig. 2C). This was consistent with the behaviour of these proteins with regards to full attachment (Fig. S3D) and suggests a mechanistic difference in their response to microtubules. Interestingly, MAD1 and BUB1 cluster as outliers in their groups, even though they are interaction partners of MAD2 and BUBR1, respectively. These differences in behaviour might be

Journal of Cell Science (2019) 132, jcs231589. doi:10.1242/jcs.231589

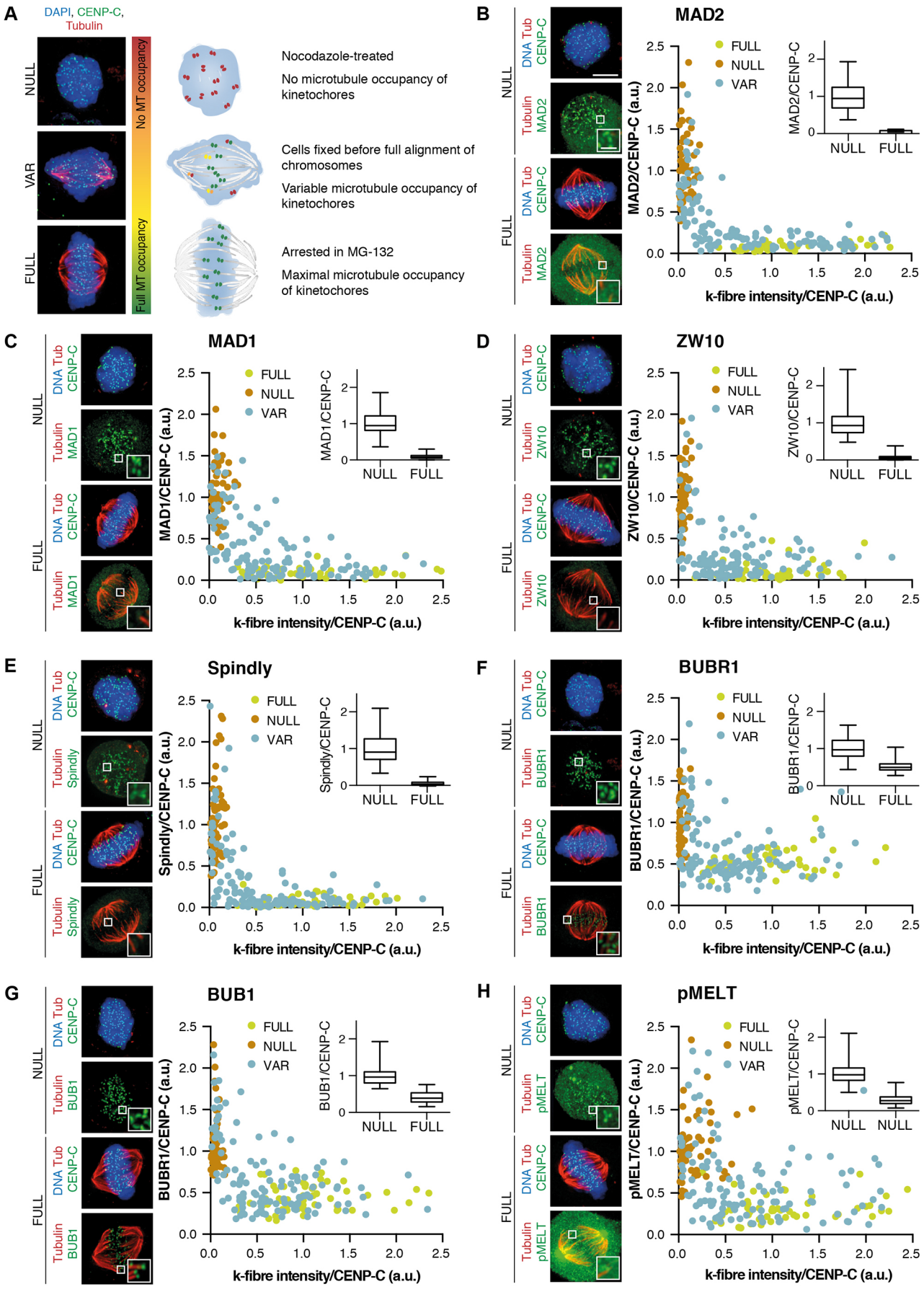

Fig. 1. See next page for legend.

Journal of Cell Science (2019) 132, jcs231589. doi:10.1242/jcs.231589

Fig. 1. SAC proteins respond to intermediate attachments states. (A) Graphic depiction of the conditions used to create a mixture of kinetochore–microtubule attachment states. (B–H) Representative images and quantifications of levels of SAC proteins on kinetochores with either a full complement of microtubules (FULL), without attachments (NULL) or with different levels of intermediate attachments (VAR). Dot plots show SAC protein levels, with data (from three biological replicates) from each experiment normalized to the median levels measured in their respective NULL conditions, and tubulin levels are normalized to the median levels measured in the FULL condition. Inset images and box plots show the NULL and FULL data only. In box plots, box represents the 25–75th percentiles, and the median is indicated. The whiskers show the range. For each protein, at least 15 kinetochores in >5 cells are measured per experiment in the FULL and NULL conditions. For the VAR condition, 42 kinetochores in >25 cells were measured per experiment. Channel colours of merged images match those of the labels. Scale bars: 5 µm in main image, 1 µm in zoom. MT, microtubule; Tub, tubulin; a.u., arbitrary units.

attributed to functions or localization mechanisms that do not rely on those interaction partners (Akera et al., 2015; Emre et al., 2011; Zhang and Nilsson, 2018; Zhang et al., 2016).

The clustering analysis predicted that members of the RZZS-MAD1-MAD2 module should behave differently in response to identical occupancy than members of BUB1-BUBR1 module when measured on the same kinetochore. Indeed, (partly) attached kinetochores with no detectable mCherry–MAD2 had a variety of BUB1 levels, and BUB1 displayed greater variability than MAD2 (Fig. 2D). In contrast, the signal intensities of BUB1 and BUBR1 on the same kinetochores of prometaphase cells were strongly correlated (Fig. 2E).

To examine whether response of the two SAC modules to intermediate attachment states indeed reflected underlying mechanistic differences, we inhibited MPS1 chemically in nocodazole-treated cells and analysed the levels of MAD1 and BUB1 as representatives of their groups. As expected, BUB1 levels declined to metaphase levels after MPS1 inhibition (Fig. 3A,B). MAD1 levels, however, remained largely unaffected, showing that MPS1 inhibition was insufficient to cause removal of MAD1 in the absence of microtubules, even though its recruitment has a substantial MPS1-dependent component (Hewitt et al., 2010; Ji et al., 2017; London et al., 2012). Removal of the two SAC modules from kinetochores is thus guided by different mechanisms.

Immature k-fibres are sufficient to silence the SAC

To understand what extent of microtubule occupancy is sufficient to silence the SAC, we next wished to experimentally tweak mean maximal occupancy. HEC1 is the major microtubule-binding protein on the kinetochore (DeLuca et al., 2002, 2005; Liu et al., 2006; McCleland et al., 2003, 2004; Wigge and Kilmartin, 2001) and its affinity for microtubules is controlled by phosphorylation of its N-terminal tail (Cheeseman et al., 2006; Wei et al., 2007). Designed combinations of phospho-site substitutions to phosphomimetic or non-phosphorylatable amino acids (aspartic acid and alanine, respectively) generates HEC1 versions with a variety of microtubule-binding affinities, which in cells results in a controlled range of mean k-fibre intensities (Zaytsev et al., 2014). We constructed cell lines expressing mutant versions of HEC1 to achieve a range of occupancy states (Fig. 4A; Fig. S4A–D). Six of these mutants (HEC1-9A, -9D, -1D, -2D, -3D and -4D) have previously been characterized extensively with regards to their microtubule affinity (Zaytsev et al., 2014, 2015); others were generated and analysed by us. Considering that single microtubules can be bound by many HEC1 molecules, our approach enabled creation of uniform HEC1 lawns with specified microtubule-binding affinities, unlike, for example, diminishing the total amount of HEC1 on kinetochores (DeLuca et al., 2002, 2003), mixing high and low affinity HEC1 species or changing microtubule dynamics artificially, which might affect other processes as well (Dudka et al., 2018). Moreover, the HEC1 mutants simulate the phosphorylation states of kinetochores during unperturbed mitosis (Zaytsev et al., 2014), providing insight into the SAC response during k-fibre maturation.

Cells expressing the HEC1 variants were analysed using time lapse imaging for their ability to silence the SAC: occupancy states that cannot silence the SAC are predicted to delay mitosis indefinitely, while those that can should allow progression. As shown in Fig. 4B,C and reported before (Etemad et al., 2015; Guimaraes et al., 2008; Zaytsev et al., 2014), cells expressing wild-type HEC1 or HEC1-9A (high microtubule affinity) were able to silence the SAC, whereas those expressing HEC1-9D (low microtubule affinity) were not. While HEC1-5D was likewise unable to silence the SAC, HEC1-4D (intermediate microtubule affinity) was proficient in SAC silencing, albeit relatively inefficiently (Fig. 4B,C). As expected, HEC1-6D, -7D and -8D were unable to silence the SAC (data not shown). Quantitative immunofluorescence showed that HEC1-4D k-fibres were on average 45% of mean maximal intensity of wild-type HEC1 cells, in line with a previous report (Zaytsev et al., 2014), and those of HEC1-5D were ∼20% (Fig. 4D,E; Fig. S1). Simultaneous live imaging of mCherry–MAD2 and eGFP–HEC1-4D showed that HEC1-4D kinetochores had shed most or all of the MAD2 by 30 min following mitotic entry (Fig. 4F). Some kinetochores, however, had retained substantial MAD2 levels after 93 min, explaining why mitotic exit was relatively inefficient in these cells compared to controls. Quantitative immuno-imaging of single attached kinetochores showed that 82% of HEC1-4D kinetochores had MAD2 levels that were as low as those of wild-type HEC1 kinetochores (Fig. 4G,H). For comparison, this was true for 30% and 0% of HEC1-5D and HEC1-9D kinetochores, respectively. These data support the hypothesis that kinetochores can inactivate SAC signalling at intermediate (∼45%) occupancy states and that SAC silencing becomes more efficient with increasing occupancy.

DISCUSSION

Each human kinetochore consists of hundreds of microtubule-binding complexes that can each recruit SAC proteins. During metaphase these kinetochores are bound by ∼20 microtubules, which shuts down SAC signalling (DeLuca et al., 2005; Guimaraes et al., 2008; McEwen et al., 2001; Wendell et al., 1993). Kinetochores are unlikely to transition from zero to a full complement of microtubules in a single step, yet there is little knowledge about SAC responses to intermediate microtubule occupancies. We show here that key SAC proteins are substantially depleted from kinetochores at ∼30% occupancy and are nearly undetectable at ∼50% occupancy or above. Our quantitative immuno-imaging of SAC protein levels in relation to microtubule intensities on single kinetochores distinguished two response types. Levels of ZW10, Spindly, MAD1 and MAD2 inversely correlated to microtubule intensities and became not or barely detectable at ∼50% occupancy. BUBR1, BUB1 and pMELT, however, although also declining strongly at low occupancy, were not sensitive to further increases in occupancy and showed variable levels. The behaviours of the members of these two groups are consistent with their mutual physical interactions, and correlate with the distinct delocalization mechanisms that have been proposed for these groups. Removal of the RZZS-MAD1-MAD2 group occurs through dynein motor activity (Caldas et al., 2015; Kim et al., 2012;

Journal of Cell Science (2019) 132, jcs231589. doi:10.1242/jcs.231589

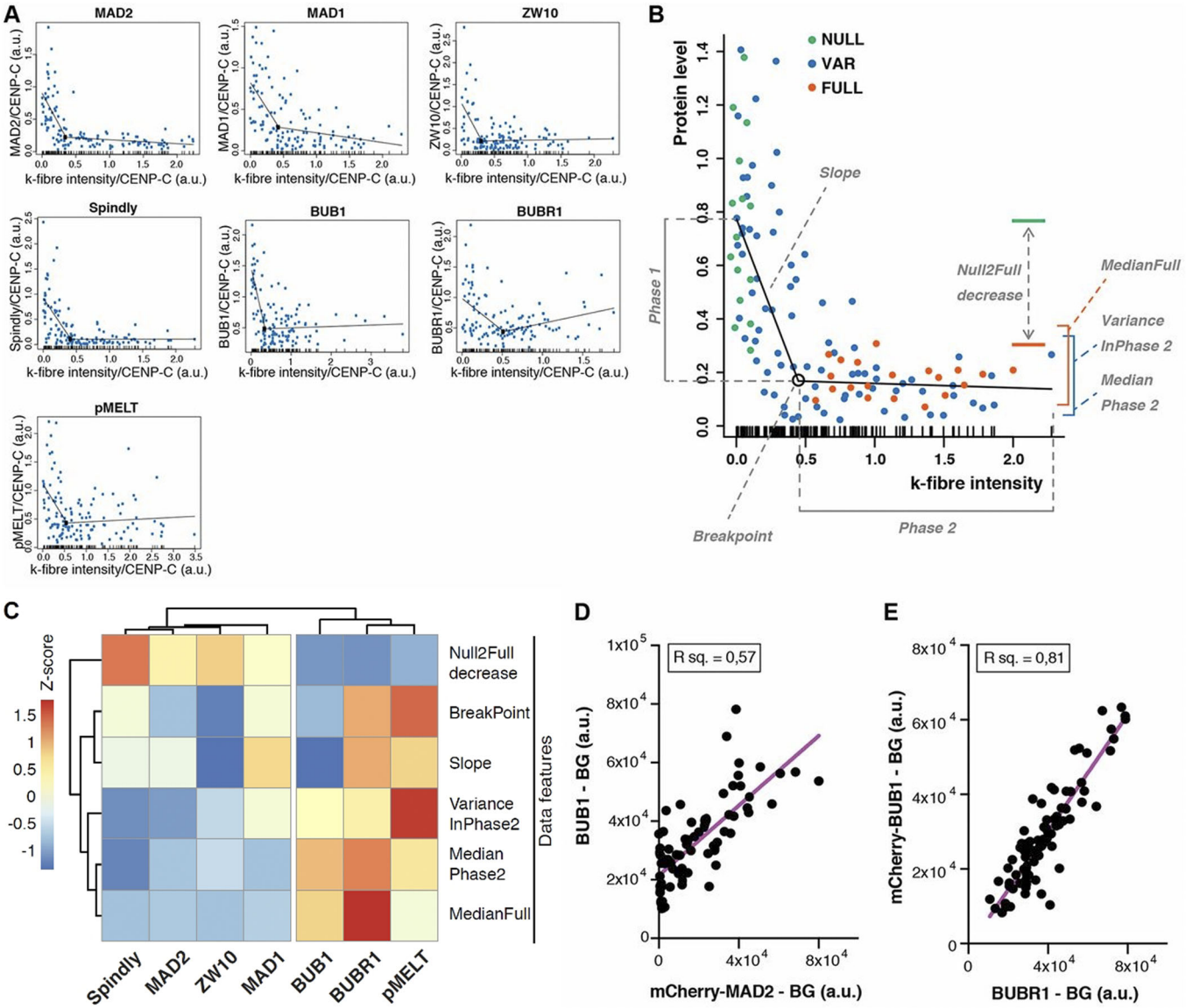

Fig. 2. Microtubule attachments evoke two distinct SAC protein responses. (A) Graphs depicting curve fits performed on the data shown in Fig. 1B–H. After pairwise linear regression, a variety of features as depicted in panel B were extracted from the fit and the data to describe the relation between k-fibre intensity and SAC protein of interest. (B) Illustration depicting the features of SAC protein localization in relation to microtubule occupancy. Features are: variance of data along the *y*-axis at the stationary stage (after breakpoint, Variance InPhase 2), rate of decrease in protein levels to minimum levels (before breakpoint, Slope), tubulin level at which proteins reach their minimum levels (Breakpoint), median of protein level at stationary stage (Median Phase 2), median protein levels in the FULL condition (MedianFull), and the decrease of FULL data set in relation to the NULL dataset (Null2Full decrease). Axes in panels A,B show protein expression and k-fibre intensity as arbitrary units. (C) Hierarchical cluster analysis of Z-score normalized features extracted from data in Fig. 1B–H as depicted in B. (D,E) Plots showing the relation between expression levels of representative SAC proteins, BUB1 and MAD2 (D), and BUB1 and BUBR1 (E), on kinetochores with different microtubule occupancy states. Cells were treated to acquire a mixture of microtubule occupancy states including the FULL and NULL conditions. Shown here are background (BG)-corrected levels of SAC proteins, plotted against corresponding BG-corrected mCherry-tagged protein expression levels. At least 72 kinetochores in >30 cells were measured. *N*=2, representative experiments are shown here.

London and Biggins, 2014; Matson and Stukenberg, 2014; Silió et al., 2015) and molecular inhibition of this mechanism does not affect BUB removal (Gassmann et al., 2010). By contrast, removal of the BUB1-BUBR1 group requires dephosphorylation by PP1 and decreased localization and activity of MPS1 (Etemad and Kops, 2016; Hiruma et al., 2015; Ji et al., 2015; Nijenhuis et al., 2014). Here, we show that inhibition of MPS1 activity in cells with no microtubules decreases BUB1 levels on unattached kinetochores, while leaving MAD1 levels mostly unaffected, supporting probable independent removal mechanisms for these SAC signalling proteins. These different responses raise the question of what attachment features (i.e. microtubule stability, tension, lateral vs end-on interaction, etc.) are recognized by either signalling module. Interestingly, MAD1 also interacts with BUB1 in an MPS1-dependent manner (Ji et al., 2017; London and Biggins, 2014; Musacchio and Salmon, 2007), and our data suggest that this interaction is either not the main MAD1-localizing mechanism in prometaphase or is insensitive to MPS1-counteracting phosphatases. Finally, although MAD1 and MAD2 form a heterotetramer, their behaviour in our analyses is not entirely overlapping. The molecular basis for this is unknown, but MAD2-independent functions for MAD1 at kinetochores have been reported (Akera et al., 2015;

Journal of Cell Science (2019) 132, jcs231589. doi:10.1242/jcs.231589

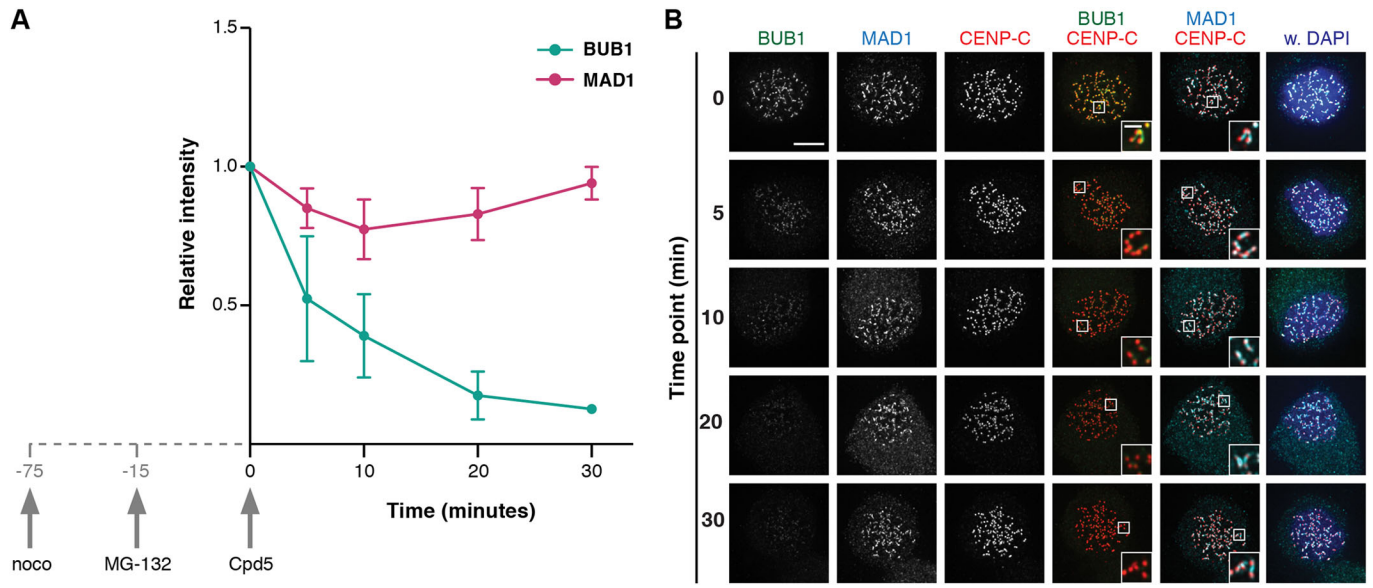

Fig. 3. Removal of the two SAC protein modules is guided by different mechanisms. Mean±s.d. protein level (relative signal intensity) plot (A) and representative images (B) showing relative decrease of MAD1 and BUB1 after chemical inhibition of MPS1 kinase with Cpd5. Cells were synchronized and pretreated for 1 h with nocodazole (noco) and 15 min with MG-132 to prevent mitotic exit prior to Cpd5 addition. Cells were fixed at indicated time points after Cpd5 addition. At least 20 cells were measured per experiment. *N*=3, representative experiment is shown here. Scale bars: 5 µm in main image, 1 µm in zoom.

Emre et al., 2011), and a pool of MAD2 depends on kinetochore-localized CDC20 (Zhang and Nilsson, 2018).

Cells in which kinetochores reach ∼45% occupancy on average (HEC1-4D) can silence the SAC and exit mitosis, while those with ∼20% occupancy (HEC1-5D) cannot. These data show that the full complement of microtubules seen on metaphase kinetochores is not strictly required for SAC silencing. The kinetochore, therefore, acts as a single unit with respect to SAC signalling; when a threshold of bound microtubules is reached, the entire unit switches off its signalling output. This has important implications for our understanding of the SAC as it suggests that the signal from hundreds of microtubule-binding complexes is quenched by only a few (∼7–10) microtubules. We envision several ways in which this can be achieved. Firstly, a few microtubules may be sufficient to pull a stiff kinetochore away from a SAC activating signal (e.g. Aurora B) originating from an inner centromere or kinetochore (Burke and Stukenberg, 2008; Santaguida and Musacchio, 2009; Saurin et al., 2011; Stukenberg and Burke, 2015). We do not favour this hypothesis, as we and others recently showed that distance between sister kinetochores or between inner and outer kinetochore is not required for SAC silencing. Secondly, a low number of microtubules may suffice to elicit a signal that sweeps the kinetochore. For example, phosphatases such as PP1 could be 'unleashed' from a site of recruitment or activation upon a threshold of microtubule binding. Concurrent with sufficient MPS1 displacement, this could switch the SAC signal to an 'off' state. It is unclear, however, how dynein-mediated removal of RZZS-MAD1-MAD2 proteins would occur in such a scenario. Thirdly, the kinetochore may be flexible, allowing only a few microtubules to engage the majority of microtubule-binding complexes and thus displace sufficient MPS1 molecules and recruit sufficient PP1 and dynein molecules to achieve substantial SAC protein delocalization. Transition to full occupancy may then be facilitated by kinetochore flexibility and many low-affinity microtubule interactions (Etemad and Kops, 2016; Hiruma et al., 2015). Fourthly, attachments may be highly dynamic, engaging and disengaging kinetochores frequently. This may allow most of the microtubule-binding complexes to briefly bind microtubules and shed SAC proteins. A sufficiently high frequency of these labile interactions could conceivably convert the kinetochore to a SAC-silenced state.

MATERIALS AND METHODS

Cell culture and transfection

HeLa and HeLa FlpIn cells (gift from the Stephen Taylor lab, University of Manchester, UK) were grown in DMEM (Sigma-Aldrich; 4.5 g glucose/l) supplemented with 8% tetracycline-free FBS (Bodingo), penicillin/streptomycin (Sigma-Aldrich; 50 µg/ml), GlutaMAX (Gibco; 5 ml), and hygromycin (200 µg/ml) or puromycin (1.6 µg/ml). Cell lines were tested frequently for contaminations. Plasmids were transfected using Fugene HD (Roche) according to the manufacturer's instructions. To generate stably integrated constructs, HeLa FlpIn cell lines were transfected with pCDNA5-constructs and pOG44 recombinase simultaneously in a 1:9 ratio (Klebig et al., 2009). Constructs were expressed by addition of 1 µg/ml doxycycline for 24 h. siHEC1 (custom; Thermo Fisher Scientific; 5′-CCCUGGGUCGUGUCAGGAA-3′) and siGAPDH (Thermo Fisher Scientific; D-001830-01-50) was transfected using HiPerfect (Qiagen) according to manufacturer's instructions.

Plasmids

pCDNA5-pEGFP-HEC1 constructs and cloning strategies are described in Nijenhuis et al. (2013). Other constructs (the 1D, 2D, 3D, 4D and 5D mutants) were made using site-directed mutagenesis by PCR.

CRISPR/Cas9 genome editing of *MAD2* and *BUB1* loci

Inserting the gene for mCherry into the endogenous loci of *MAD2* and *BUB1* was performed using a self-cloning CRISPR strategy (Arbab et al., 2015). In brief: 3×FLAG-spCas9 was subcloned from spCas9-BLAST to pcDNA3-MCS-IRES-PURO using NdeI/EcoRI restriction digestion to allow selection for spCas9 expression in HeLa FLPin cells. To generate HA-mCherry, pcDNA3Zeo-CyclinB-mCherry (Kuijt et al., 2014) was used as template and amplified by PCR using forward (5′-AAGCTTTAC-CCGTACGACGTGCCAGATTACGCTGTGAGCAAGGGCGAGGAGG-3′) and reverse (5′-gcgccgTCTAGATCCGCAGCCACCGCCAGATCCG-CCCTTGTACAGCTCGTCCATGC-3′) primers. The PCR fragment was digested with HindIII/XbaI and ligated into pcDNA3.0 via HindIII/XbaI.

Journal of Cell Science (2019) 132, jcs231589. doi:10.1242/jcs.231589

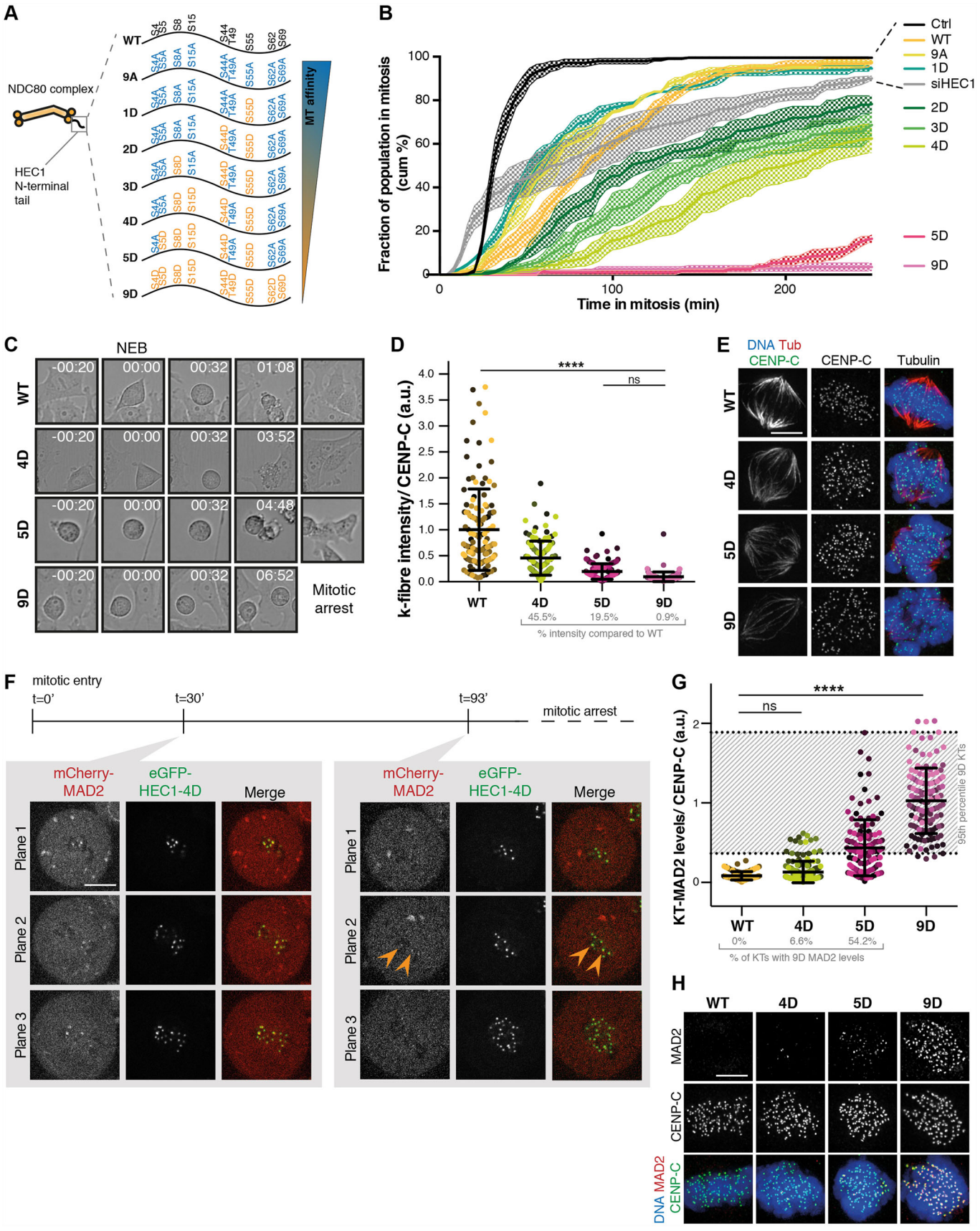

Fig. 4. See next page for legend.

Journal of Cell Science (2019) 132, jcs231589. doi:10.1242/jcs.231589

Fig. 4. Immature k-fibres are sufficient to silence the SAC. (A) Overview of the mutants used in this study. The HEC1 variants have phosphomimetic (aspartic acid, D) or non-phosphorylatable (aspartame, A) amino acid substitutions in all nine known phosphorylation sites in the N-terminal tail of HEC1. (B,C) Quantification (B) and representative stills (C) of unperturbed mitotic duration in cells expressing variants of HEC1. At least 50 cells were scored per condition in three independent experiments. Shown here are the mean of three experiments (continuous line) and s.e.m. (dotted area). cum %, cumulative percentage; WT, wild type; Ctrl, control. (D,E) Quantification (D) and representative images (E) of the intensity of k-fibres in cells expressing indicated HEC1 variants. Cells were arrested in metaphase for 2 h prior to fixation to allow maximum microtubule occupancy. Each data point in D represents one kinetochore or k-fibre. >118 kinetochores of >5 cells were scored per cell line and different shades of the same colour indicate different cells. For statistical analysis, a one-way ANOVA test was performed. ****P<0.0001; ns, not significant. a.u., arbitrary units. Channel colours of merged images in E match those of the labels. N=2, representative experiment is shown here. Scale bar: 5 µm. (F) Representative stills of cell in mitosis simultaneously expressing mCherry–MAD2 from its endogenous locus and eGFP–HEC1-4D. Cells were released from a G2/M-block to track mitotic entry and followed for ∼100 min. Shown here are selected planes (3/16) at two time points. Arrowheads indicate two MAD2-positive kinetochores at t=93 min, MAD2 was undetectable on other kinetochores. (G,H) Quantification (G) and representative images (H) of the intensity of kinetochore (KT)-MAD2 in cells expressing indicated HEC1 variants. Cells were arrested in metaphase for 2 h prior to fixation to allow maximum microtubule occupancy. Each data point in G represents one kinetochore or k-fibre. >118 kinetochores of >5 cells were scored per cell line and different shades of the same colour indicate different cells. For statistical analysis, a one-way ANOVA test was performed. ****P<0.0001; ns, not significant. In H, channel colours of merged images match those of the labels. N=2, representative experiment is shown here. Scale bar: 5 µm. The mean±s.d. is shown in B and G.

To create the homology arms, three consecutive PCR-amplifications were done on HA-mCherry template to create MAD2 (120 bp 5′ of ATG and 120 bp 3′) or BUB1 (119 bp 5′ of ATG and 124 bp 3′). spCas9 was directed to MAD2 using sgRNA: 5′-GAGCTGCAGCGCCATGGCC-3′, or BUB1 using 5′-GTCCTCTGGCCATGGACACCC-3′. Both homology arms and sgRNA template were subcloned into pJet1.2 (Thermo Fisher Scientific) and sequence verified before PCR fragments were generated for transfection.

To generate HeLa FlpIn cells expressing endogenous tagged MAD2 or BUB1, cells were transfected with 1.5 µg spCas9-IRES-PURO, 1.5 µg sgPAL7-Hygro, 3 µg homology PCR template and 3 µg sgRNA PCR template at a ratio 1:3 DNA:Lipofectamine LTX (Thermo Fisher Scientific). 24 h after transfection, 1 µg/ml puromycin and 200 µg/ml hygromycin B were used for 48 h, after which cells were grown until confluence in a 10 cm Petri dish. HeLa FlpIn cells were subsequently FACS-sorted as single cells using a BD FACSAria FUSION (640 nm excitation laser, autofluorescence 670 nm/30 vs 651 nm excitation laser, 610 nm/20 mCherry channels, 100 µm nozzle, 2.0 flowrate). Clones were verified to have correct labelling of MAD2 or BUB1 by PCR on genomic DNA, western blotting and live-cell immunofluorescence microscopy.

Knockdown and reconstitution experiments

To knock down and reconstitute HEC1 in HeLa FLpIn cell lines, cells were transfected with 40 nM siRNA against HEC1 or mock siRNA and arrested in early S phase for 24 h by addition of thymidine (2 mM). Cells were then allowed cell cycle re-entry by washing the cells once with appropriate media. 8 h after thymidine release, cells were treated with doxycycline (1 µg/ml), arrested again using thymidine and incubated with both reagents for 16 h after which they were released from thymidine and further processed. Cells processed for immunofluorescence imaging of SAC proteins and k-fibres were released from thymidine in CDK1 inhibitor RO-3306 (5 µM) and incubated for 8 h or more. Subsequently, cells were washed three times with warm media, incubated between each wash for 5 min at 37°C, and incubated for 120 min with nocodazole (3.3 µM, 'NULL' condition), or MG-132 (5 µM, 'FULL' condition). Next, cells were fixed and processed appropriately. To fix cells before all kinetochores had reached full occupancy (the 'VAR' condition), cells were fixed and processed 25 min after release from a G2/M-boundary block by RO-3306 (5 µM). For immunofluorescence imaging of cells expressing HEC1 variants, cells were treated with MG-132 (5 µM) for 120 min prior to fixation. To follow BUB1 and MAD1 levels in time after MPS1 inhibition, cells were synchronized with thymidine and blocked at the G2/M-boundary using RO-3306 (5 µM). Cells were then released from RO-3306 inhibition using nocodazole (3,3 µM). After 1 h nocodazole block, cells were treated with MG-132 for 15 min, after which Cpd5 (250 nM) was added to inhibit MPS1 activity.

Live-cell imaging

For live-cell imaging experiments, cells were plated in 24-well plates (Greiner Bio-One), and subjected to DIC microscopy on a Nikon Ti-E motorized microscope equipped with a Zyla 4.2 Mpx sCMOS camera (Andor). A 20×0.45 NA objective lens (Nikon) was used. Cells were kept at 37°C and 5% CO_2 using a cage incubator and Boldline temperature/CO_2 controller (OKO-Lab). Images were acquired every 4 min at 2×2 binning and processed by Nikon Imaging Software (NIS). Analysis of live-cell imaging experiments was carried out with ImageJ software and time in mitosis was defined as the time between nuclear envelope breakdown and anaphase onset or cell flattening.

Live-cell imaging of mCherry-tagged MAD2 and BUB1 in single cells was performed on a Nikon Time-Lapse system (Applied Precision/GE Healthcare) equipped with a Coolsnap HQ2 CCD camera (Photometrics) and Insight solid-state illumination (Applied Precision/GE Healthcare). Cells were plated in 8-well plates (µ-Slide 8-well, Ibidi) and imaged in a heated chamber (37°C and 5% CO_2) using a 60×/1.42 NA or 100×/1.4 NA UPlanSApo objective (Olympus) at 2×2 binning. Images were acquired every 15 s (for the mCherry–MAD2 cells), or 1 min (for the mCherry–BUB1 cells), and deconvolved using standard settings in SoftWorx (Applied Precision/GE Healthcare) software. Multiple z-layers were acquired and projected to a single layer by maximum intensity projection. For simultaneous imaging of GFP (HEC1) and mCherry–MAD2, the same system was used. Cells were plated in 8-well plates (µ-Slide 8-well, Ibidi), treated with siRNA, thymidine and RO-3306 as described above. Images were acquired 30 and 60 min after mitotic entry, and then every three minutes.

Immunofluorescence and image quantification

For fixed-cell immunofluorescence microscopy, cells plated on round 12-mm coverslips (no. 1.5) were pre-extracted with 37°C 0.1% Triton X-100 in PEM (100 mM PIPES pH 6.8, 1 mM $MgCl_2$, 5 mM EGTA) for ∼45 s before fixation (with 4% paraformaldehyde) for 10 min. Coverslips were washed twice with cold PBS and blocked with 3% BSA in PBS for 16 h at 4°C, incubated with primary antibodies for 16 h at 4°C, washed four times with PBS containing 0.1% Triton X-100, and incubated with secondary antibodies for an additional hour at room temperature. Coverslips were then washed twice with PBS/0.1% Triton X-100, incubated with DAPI for 2 min, washed again twice with PBS and mounted using Prolong Gold antifade (Invitrogen). For cold-shock experiments, cells were placed on ice water in 500 µl media for 8 min prior to pre-extraction and fixation with the appropriate buffers.

All images were acquired on a deconvolution system (DeltaVision Elite; Applied Precision/GE Healthcare) with a 100×/1.40 NA UPlanSApo objective (Olympus) using SoftWorx 6.0 software (Applied Precision/GE Healthcare). Deconvolution is applied to all images and maximum projection is shown in figures, except for Fig. S1A, which is a sum-projection image, and Fig. 4F in which single planes are shown. For quantification of immunostaining, all images of simultaneously stained experiments were acquired with identical illumination settings. For analysis of the HEC1 mutant-expressing cell lines, cells expressing comparable levels of exogenous protein were selected for analysis and analysed using ImageJ. For measurement of protein levels and k-fibre intensities on single kinetochores, kinetochores were selected in maximum-projection images. The 7–8 slices that contained a single kinetochore and corresponding k-fibre were selected and sum-projection images were used for quantification. Line plots were used to determine the highest intensity at kinetochores and/or

k-fibres and local background was subtracted from these values (Fig. S1). The same method was applied to determine protein levels, k-fibre intensity and CENP-C levels. K-fibre and protein measurements were normalized to CENP-C to correct for biological and technical variation between kinetochores. Further normalization steps included normalization of k-fibre levels to the median levels measured in FULL conditions, and normalization of protein levels to the levels measured for the median of the same protein in the NULL conditions.

Sample size for live imaging and immunofluorescence experiments was chosen based on common practice in the field

Data analysis

Data analysis was performed in R (3.3.2) using the pheatmap (1.0.8, CRAN), MarkdownReports (2.5, doi:10.5281/zenodo.594683) packages. Raw measurements per kinetochore were normalized as described in 'Immunofluorescence and image quantification'.

To quantify features of individual occupancy response curves in transient (left) and steady (right) phase separately, piecewise linear regression was applied, where a breakpoint separates the two phases. Each feature is extracted from either the FULL, NULL or the VAR datasets as denoted. These features are: VarianceInPhase2 (variance in protein concentration in the steady phase, right of the split point), MedianPhase2 (median protein concentration in the steady phase), Null2Full decrease (relative protein decrease between the two conditions defined as the ratio of median protein levels NULL over FULL attachment, corresponds to data presented in insets in Fig. 1B–H), MedianFull (median protein levels in the full condition), Breakpoint (x- or tubulin-coordinate of the split point in the piecewise linear regression), and Slope (slope of the fitted line in the transient phase, left of the split point).

To investigate variance across proteins at full attachment, measured values were tested for normality. Based on these results, Levene's test was used to compare variances.

Immunoblotting

Cells were treated as described above and entered mitosis in the presence of nocodazole. Cells were collected and lysed in Laemmli lysis buffer (4% SDS, 120 mM Tris pH 6.8, 20% glycerol). Lysates were processed for SDS-PAGE and transferred to nitrocellulose membranes for immunoblotting. Immunoblotting was performed using standard protocols. Visualization of signals was performed on a scanner (Amersham Imager 600) using enhanced chemiluminescense.

Antibodies

The following primary antibodies were used for immunofluorescence imaging: CENP-C (guinea pig polyclonal, 1:2000; Sigma-Aldrich, PD 030), α-tubulin (mouse monoclonal, 1:10,000; Sigma-Aldrich, T5168), HEC1 (mouse monoclonal 9G3, 1:2000; Abcam, Ab-3613), GFP (custom rabbit polyclonal raised against full-length GFP as antigen, 1:10,000; Jelluma et al., 2008), GFP (mouse monoclonal, 1:1000; Roche, 12-814-460-001), MAD2 (custom rabbit polyclonal raised against full-length 6×His-tagged MAD2 as antigen, 1:2000; Sliedrecht et al., 2010), BubR1 (rabbit polyclonal, 1:1000; Bethyl, A300-386 A), BUB1 (rabbit polyclonal, 1:1000; Bethyl, A300-373 A-1), Spindly (rabbit polyclonal, 1:1000; Bethyl, A301-354A), ZW10 (rabbit polyclonal, 1:1000; Abcam, ab21582), MAD1 (rabbit polyclonal, 1:1000; Santa Cruz, cat. no. sc-67337), RFP (rat monoclonal, 1:1000; Chromotek, 5F8) GFP-Booster (Atto 488, 1:500; Chromotek, gba488). Secondary antibodies (Invitrogen Molecular Probes, all used at 1:600) were highly cross-absorbed goat anti-guinea pig Alexa Fluor 647 (A21245), anti-rat Alexa Fluor 568 (A11077), goat anti-rabbit Alexa Fluor 488 (A11034) and 568 (A11036), and anti-mouse Alexa Fluor 488 (A11029) and 568 (A11031).

The following primary antibodies were used for immunoblotting: HEC1 (mouse monoclonal, 1:1000; Abcam, ab3613), α-tubulin (mouse monoclonal, 1:10.000; Sigma, T5168), mCherry (rabbit polyclonal, 1:1000; Abcam, ab167453), BUB1 (rabbit polyclonal, 1:1000; Bethyl, A300-373 A-1), MAD2 (custom rabbit polyclonal raised against full-length 6xHis-tagged MAD2 as antigen, 1:2000; Sliedrecht et al., 2010). Secondary antibodies were: goat anti-rabbit IgG, HRP-conjugate (1:10.000; Bioke, #7074) and goat anti-mouse IgG, HRP-conjugate (1:10.000; Bio-Rad, #1706516).

Acknowledgements

We thank Jennifer DeLuca (Colorado State University, Fort Collins, CO) for reagents, members of the Kops lab for discussions, and Sophie Dumont and Jonathan Kuhn (University of California, San Fransisco, CA) for sharing unpublished data.

Competing interests

The authors declare no competing or financial interests.

Author contributions

Conceptualization: B.E., G.J.P.L.K.; Methodology: B.E., A.V., T.E.F.K., C.S.; Software: A.V.; Validation: B.E., A.V., T.E.F.K., C.S.; Formal analysis: A.V., T.E.F.K., C.S.; Investigation: B.E., T.E.F.K., C.S.; Data curation: B.E., C.S.; Writing - original draft: B.E., G.J.P.L.K.; Writing - review & editing: B.E., A.V., T.E.F.K., C.S., G.J.P.L.K.; Visualization: B.E., T.E.F.K., C.S.; Supervision: A.v.O., G.J.P.L.K.; Project administration: A.v.O., G.J.P.L.K.; Funding acquisition: A.v.O., G.J.P.L.K.

Funding

This study was supported by Oncode Institute, which is partly funded by KWF Kankerbestrijding (Dutch Cancer Society), and by Nederlandse Organisatie voor Wetenschappelijk Onderzoek (Netherlands Organisation for Scientific Research) (NWO-Vici 865.12.004).

Data availability

The source code for the analysis and raw quantification data is available 'as-is' under GNU GPLv3 at https://github.com/vertesy/Kinetochore.

Supplementary information

Supplementary information available online at
http://jcs.biologists.org/lookup/doi/10.1242/jcs.231589.supplemental

References

Akera, T., Goto, Y., Sato, M., Yamamoto, M. and Watanabe, Y. (2015). Mad1 promotes chromosome congression by anchoring a kinesin motor to the kinetochore. *Nat. Cell Biol.* **17**, 1124-1133. doi:10.1038/ncb3219

Arbab, M., Srinivasan, S., Hashimoto, T., Geijsen, N. and Sherwood, R. I. (2015). Cloning-free CRISPR. *Stem Cell Rep.* **5**, 908-917. doi:10.1016/j.stemcr.2015.09.022

Auckland, P., Clarke, N. I., Royle, S. J. and McAinsh, A. D. (2017). Congressing kinetochores progressively load Ska complexes to prevent force-dependent detachment. *J. Cell Biol.* **216**, 1623-1639. doi:10.1083/jcb.201607096

Ballister, E. R., Riegman, M. and Lampson, M. A. (2014). Recruitment of Mad1 to metaphase kinetochores is sufficient to reactivate the mitotic checkpoint. *J. Cell Biol.* **204**, 901-908. doi:10.1083/jcb.201311113

Barisic, M., Sohm, B., Mikolcevic, P., Wandke, C., Rauch, V., Ringer, T., Hess, M., Bonn, G. and Geley, S. (2010). Spindly/CCDC99 is required for efficient chromosome congression and mitotic checkpoint regulation. *Mol. Biol. Cell* **21**, 1968-1981. doi:10.1091/mbc.e09-04-0356

Bomont, P., Maddox, P., Shah, J. V., Desai, A. B. and Cleveland, D. W. (2005). Unstable microtubule capture at kinetochores depleted of the centromere-associated protein CENP-F. *EMBO J.* **24**, 3927-3939. doi:10.1038/sj.emboj.7600848

Burke, D. J. and Stukenberg, P. T. (2008). Linking kinetochore-microtubule binding to the spindle checkpoint. *Dev. Cell* **14**, 474-479. doi:10.1016/j.devcel.2008.03.015

Caldas, G. V., Lynch, T. R., Anderson, R., Afreen, S., Varma, D. and DeLuca, J. G. (2015). The RZZ complex requires the N-terminus of KNL1 to mediate optimal Mad1 kinetochore localization in human cells. *Open Biol.* **5**, 150160. doi:10.1098/rsob.150160

Chan, Y. W., Fava, L. L., Uldschmid, A., Schmitz, M. H. A., Gerlich, D. W., Nigg, E. A. and Santamaria, A. (2009). Mitotic control of kinetochore-associated dynein and spindle orientation by human Spindly. *J. Cell Biol.* **185**, 859-874. doi:10.1083/jcb.200812167

Chao, W. C. H., Kulkarni, K., Zhang, Z., Kong, E. H. and Barford, D. (2012). Structure of the mitotic checkpoint complex. *Nature* **484**, 208-213. doi:10.1038/nature10896

Cheeseman, I. M., Chappie, J. S., Wilson-Kubalek, E. M. and Desai, A. (2006). The conserved KMN network constitutes the core microtubule-binding site of the kinetochore. *Cell* **127**, 983-997. doi:10.1016/j.cell.2006.09.039

Collin, P., Nashchekina, O., Walker, R. and Pines, J. (2013). The spindle assembly checkpoint works like a rheostat rather than a toggle switch. *Nat. Cell Biol.* **15**, 1378-1385. doi:10.1038/ncb2855

de Wolf, B. and Kops, G. J. P. L. (2017). Kinetochore malfunction in human pathologies. *Adv. Exp. Med. Biol.* **1002**, 69-91. doi:10.1007/978-3-319-57127-0_4

DeLuca, J. G. and Musacchio, A. (2012). Structural organization of the kinetochore-microtubule interface. *Curr. Opin. Cell Biol.* **24**, 48-56. doi:10.1016/j.ceb.2011.11.003

DeLuca, J. G., Moree, B., Hickey, J. M., Kilmartin, J. V. and Salmon, E. D. (2002). hNuf2 inhibition blocks stable kinetochore-microtubule attachment and

induces mitotic cell death in HeLa cells. *J. Cell Biol.* **159**, 549-555. doi:10.1083/jcb.200208159

DeLuca, J. G., Howell, B. J., Canman, J. C., Hickey, J. M., Fang, G. and Salmon, E. D. (2003). Nuf2 and Hec1 are required for retention of the checkpoint proteins Mad1 and Mad2 to kinetochores. *Curr. Biol.* **13**, 2103-2109. doi:10.1016/j.cub.2003.10.056

DeLuca, J. G., Dong, Y., Hergert, P., Strauss, J., Hickey, J. M., Salmon, E. D. and McEwen, B. F. (2005). Hec1 and nuf2 are core components of the kinetochore outer plate essential for organizing microtubule attachment sites. *Mol. Biol. Cell* **16**, 519-531. doi:10.1091/mbc.e04-09-0852

Dudka, D., Noatynska, A., Smith, C. A., Liaudet, N., McAinsh, A. D. and Meraldi, P. (2018). Complete microtubule-kinetochore occupancy favours the segregation of merotelic attachments. *Nat. Commun.* **9**, 2042. doi:10.1038/s41467-018-04427-x

Duijf, P. H. G., Schultz, N. and Benezra, R. (2013). Cancer cells preferentially lose small chromosomes. *Int. J. Cancer* **132**, 2316-2326. doi:10.1002/ijc.27924

Emre, D., Terracol, R., Poncet, A., Rahmani, Z. and Karess, R. E. (2011). A mitotic role for Mad1 beyond the spindle checkpoint. *J. Cell Sci.* **124**, 1664-1671. doi:10.1242/jcs.081216

Espeut, J., Lara-Gonzalez, P., Sassine, M., Shiau, A. K., Desai, A. and Abrieu, A. (2015). Natural loss of Mps1 kinase in nematodes uncovers a role for polo-like kinase 1 in spindle checkpoint initiation. *Cell Rep.* **12**, 58-65. doi:10.1016/j.celrep.2015.05.039

Etemad, B. and Kops, G. J. P. L. (2016). Attachment issues: kinetochore transformations and spindle checkpoint silencing. *Curr. Opin. Cell Biol.* **39**, 101-108. doi:10.1016/j.ceb.2016.02.016

Etemad, B., Kuijt, T. E. F. and Kops, G. J. P. L. (2015). Kinetochore-microtubule attachment is sufficient to satisfy the human spindle assembly checkpoint. *Nat. Commun.* **6**, 8987. doi:10.1038/ncomms9987

Funabiki, H. and Wynne, D. J. (2013). Making an effective switch at the kinetochore by phosphorylation and dephosphorylation. *Chromosoma* **122**, 135-158. doi:10.1007/s00412-013-0401-5

Gassmann, R., Essex, A., Hu, J.-S., Maddox, P. S., Motegi, F., Sugimoto, A., O'Rourke, S. M., Bowerman, B., McLeod, I., Yates, J. R. et al. (2008). A new mechanism controlling kinetochore-microtubule interactions revealed by comparison of two dynein-targeting components: SPDL-1 and the Rod/Zwilch/Zw10 complex. *Genes Dev.* **22**, 2385-2399. doi:10.1101/gad.1687508

Gassmann, R., Holland, A. J., Varma, D., Wan, X., Civril, F., Cleveland, D. W., Oegema, K., Salmon, E. D. and Desai, A. (2010). Removal of Spindly from microtubule-attached kinetochores controls spindle checkpoint silencing in human cells. *Genes Dev.* **24**, 957-971. doi:10.1101/gad.1886810

Guimaraes, G. J., Dong, Y., McEwen, B. F. and DeLuca, J. G. (2008). Kinetochore-microtubule attachment relies on the disordered N-terminal tail domain of Hec1. *Curr. Biol.* **18**, 1778-1784. doi:10.1016/j.cub.2008.08.012

Hanahan, D. and Weinberg, R. A. (2011). Hallmarks of cancer: the next generation. *Cell* **144**, 646-674. doi:10.1016/j.cell.2011.02.013

Herzog, F., Primorac, I., Dube, P., Lenart, P., Sander, B., Mechtler, K., Stark, H. and Peters, J.-M. (2009). Structure of the anaphase-promoting complex/cyclosome interacting with a mitotic checkpoint complex. *Science* **323**, 1477-1481. doi:10.1126/science.1163300

Hewitt, L., Tighe, A., Santaguida, S., White, A. M., Jones, C. D., Musacchio, A., Green, S. and Taylor, S. S. (2010). Sustained Mps1 activity is required in mitosis to recruit O-Mad2 to the Mad1-C-Mad2 core complex. *J. Cell Biol.* **190**, 25-34. doi:10.1083/jcb.201002133

Hiruma, Y., Sacristan, C., Pachis, S. T., Adamopoulos, A., Kuijt, T., Ubbink, M., von Castelmur, E., Perrakis, A. and Kops, G. J. P. L. (2015). Competition between MPS1 and microtubules at kinetochores regulates spindle checkpoint signaling. *Science* **348**, 1264-1267. doi:10.1126/science.aaa4055

Hoffman, D. B., Pearson, C. G., Yen, T. J., Howell, B. J. and Salmon, E. D. (2001). Microtubule-dependent changes in assembly of microtubule motor proteins and mitotic spindle checkpoint proteins at PtK1 kinetochores. *Mol. Biol. Cell* **12**, 1995-2009. doi:10.1091/mbc.12.7.1995

Howell, B. J., McEwen, B. F., Canman, J. C., Hoffman, D. B., Farrar, E. M., Rieder, C. L. and Salmon, E. D. (2001). Cytoplasmic dynein/dynactin drives kinetochore protein transport to the spindle poles and has a role in mitotic spindle checkpoint inactivation. *J. Cell Biol.* **155**, 1159-1172. doi:10.1083/jcb.200105093

Howell, B. J., Moree, B., Farrar, E. M., Stewart, S., Fang, G. and Salmon, E. D. (2004). Spindle checkpoint protein dynamics at kinetochores in living cells. *Curr. Biol.* **14**, 953-964. doi:10.1016/j.cub.2004.05.053

Ito, D., Saito, Y. and Matsumoto, T. (2012). Centromere-tethered Mps1 pombe homolog (Mph1) kinase is a sufficient marker for recruitment of the spindle checkpoint protein Bub1, but not Mad1. *Proc. Natl. Acad. Sci. USA* **109**, 209-214. doi:10.1073/pnas.1114647109

Jelluma, N., Brenkman, A. B., McLeod, I., Yates, J. R., Cleveland, D. W., Medema, R. H. and Kops, G. J. P. L. (2008). Chromosomal instability by inefficient Mps1 auto-activation due to a weakened Mitotic Checkpoint and lagging chromosomes. *PLoS ONE* **3**, e2415. doi:10.1371/journal.pone.0002415

Jelluma, N., Dansen, T. B., Sliedrecht, T., Kwiatkowski, N. P. and Kops, G. J. P. L. (2010). Release of Mps1 from kinetochores is crucial for timely anaphase onset. *J. Cell Biol.* **191**, 281-290. doi:10.1083/jcb.201003038

Ji, Z., Gao, H. and Yu, H. (2015). Kinetochore attachment sensed by competitive Mps1 and microtubule binding to Ndc80C. *Science* **348**, 1260-1264. doi:10.1126/science.aaa4029

Ji, Z., Gao, H., Jia, L., Li, B. and Yu, H. (2017). A sequential multi-target Mps1 phosphorylation cascade promotes spindle checkpoint signaling. *eLife* **6**, e22513. doi:10.7554/eLife.22513

Kim, S., Sun, H., Tomchick, D. R., Yu, H. and Luo, X. (2012). Structure of human Mad1 C-terminal domain reveals its involvement in kinetochore targeting. *Proc. Natl. Acad. Sci. USA* **109**, 6549-6554. doi:10.1073/pnas.1118210109

Klebig, C., Korinth, D. and Meraldi, P. (2009). Bub1 regulates chromosome segregation in a kinetochore-independent manner. *J. Cell Biol.* **185**, 841-858. doi:10.1083/jcb.200902128

Kops, G. J. P. L., Kim, Y., Weaver, B. A. A., Mao, Y., McLeod, I., Yates, J. R., Tagaya, M. and Cleveland, D. W. (2005). ZW10 links mitotic checkpoint signaling to the structural kinetochore. *J. Cell Biol.* **169**, 49-60. doi:10.1083/jcb.200411118

Krenn, V., Overlack, K., Primorac, I., van Gerwen, S. and Musacchio, A. (2014). KI motifs of human Knl1 enhance assembly of comprehensive spindle checkpoint complexes around MELT repeats. *Curr. Biol.* **24**, 29-39. doi:10.1016/j.cub.2013.11.046

Kuhn, J. and Dumont, S. (2017). Spindle assembly checkpoint satisfaction occurs via end-on but not lateral attachments under tension. *J. Cell Biol.* **216**, 1533-1542. doi:10.1083/jcb.201611104

Kuijt, T. E. F., Omerzu, M., Saurin, A. T. and Kops, G. J. P. L. (2014). Conditional targeting of MAD1 to kinetochores is sufficient to reactivate the spindle assembly checkpoint in metaphase. *Chromosoma* **123**, 471-480. doi:10.1007/s00412-014-0458-9

Kulukian, A., Han, J. S. and Cleveland, D. W. (2009). Unattached kinetochores catalyze production of an anaphase inhibitor that requires a Mad2 template to prime Cdc20 for BubR1 binding. *Dev. Cell* **16**, 105-117. doi:10.1016/j.devcel.2008.11.005

Liu, X. and Winey, M. (2012). The MPS1 family of protein kinases. *Annu. Rev. Biochem.* **81**, 561-585. doi:10.1146/annurev-biochem-061611-090435

Liu, S.-T., Rattner, J. B., Jablonski, S. A. and Yen, T. J. (2006). Mapping the assembly pathways that specify formation of the trilaminar kinetochore plates in human cells. *J. Cell Biol.* **175**, 41-53. doi:10.1083/jcb.200606020

London, N. and Biggins, S. (2014). Mad1 kinetochore recruitment by Mps1-mediated phosphorylation of Bub1 signals the spindle checkpoint. *Genes Dev.* **28**, 140-152. doi:10.1101/gad.233700.113

London, N., Ceto, S., Ranish, J. A. and Biggins, S. (2012). Phosphoregulation of Spc105 by Mps1 and PP1 regulates Bub1 localization to kinetochores. *Curr. Biol.* **22**, 900-906. doi:10.1016/j.cub.2012.03.052

Maldonado, M. and Kapoor, T. M. (2011). Constitutive Mad1 targeting to kinetochores uncouples checkpoint signalling from chromosome biorientation. *Nat. Cell Biol.* **13**, 475-482. doi:10.1038/ncb2223

Martinez-Exposito, M. J., Kaplan, K. B., Copeland, J. and Sorger, P. K. (1999). Retention of the BUB3 checkpoint protein on lagging chromosomes. *Proc. Natl. Acad. Sci. USA* **96**, 8493-8498. doi:10.1073/pnas.96.15.8493

Matson, D. R. and Stukenberg, P. T. (2014). CENP-I and Aurora B act as a molecular switch that ties RZZ/Mad1 recruitment to kinetochore attachment status. *J. Cell Biol.* **205**, 541-554. doi:10.1083/jcb.201307137

McCleland, M. L., Gardner, R. D., Kallio, M. J., Daum, J. R., Gorbsky, G. J., Burke, D. J. and Stukenberg, P. T. (2003). The highly conserved Ndc80 complex is required for kinetochore assembly, chromosome congression, and spindle checkpoint activity. *Genes Dev.* **17**, 101-114. doi:10.1101/gad.1040903

McCleland, M. L., Kallio, M. J., Barrett-Wilt, G. A., Kestner, C. A., Shabanowitz, J., Hunt, D. F., Gorbsky, G. J. and Stukenberg, P. T. (2004). The vertebrate Ndc80 complex contains Spc24 and Spc25 homologs, which are required to establish and maintain kinetochore-microtubule attachment. *Curr. Biol.* **14**, 131-137. doi:10.1016/j.cub.2003.12.058

McEwen, B. F., Chan, G. K. T., Zubrowski, B., Savoian, M. S., Sauer, M. T. and Yen, T. J. (2001). CENP-E is essential for reliable bioriented spindle attachment, but chromosome alignment can be achieved via redundant mechanisms in mammalian cells. *Mol. Biol. Cell* **12**, 2776-2789. doi:10.1091/mbc.12.9.2776

Meadows, J. C., Shepperd, L. A., Vanoosthuyse, V., Lancaster, T. C., Sochaj, A. M., Buttrick, G. J., Hardwick, K. G. and Millar, J. B. A. (2011). Spindle checkpoint silencing requires association of PP1 to both Spc7 and kinesin-8 motors. *Dev. Cell* **20**, 739-750. doi:10.1016/j.devcel.2011.05.008

Musacchio, A. and Desai, A. (2017). A molecular view of kinetochore assembly and function. *Biology (Basel)*. **6**, 5. doi:10.3390/biology6010005

Musacchio, A. and Salmon, E. D. (2007). The spindle-assembly checkpoint in space and time. *Nat. Rev. Mol. Cell Biol.* **8**, 379-393. doi:10.1038/nrm2163

Nijenhuis, W., von Castelmur, E., Littler, D., De Marco, V., Tromer, E., Vleugel, M., van Osch, M. H. J., Snel, B., Perrakis, A. and Kops, G. J. P. L. (2013). A TPR domain-containing N-terminal module of MPS1 is required for its kinetochore localization by Aurora B. *J. Cell Biol.* **201**, 217-231. doi:10.1083/jcb.201210033

Nijenhuis, W., Vallardi, G., Teixeira, A., Kops, G. J. P. L. and Saurin, A. T. (2014). Negative feedback at kinetochores underlies a responsive spindle checkpoint signal. *Nat. Cell Biol.* **16**, 1257-1264. doi:10.1038/ncb3065

Nixon, F. M., Gutiérrez-Caballero, C., Hood, F. E., Booth, D. G., Prior, I. A., Royle, S. J., Mattaj, I., Reichel, J., Porrati, P., Pellegatta, S. et al. (2015). The

mesh is a network of microtubule connectors that stabilizes individual kinetochore fibers of the mitotic spindle. *eLife* **4**, 2443-2451. doi:10.7554/eLife.07635

Overlack, K., Primorac, I., Vleugel, M., Krenn, V., Maffini, S., Hoffmann, I., Kops, G. J. P. L. and Musacchio, A. (2015). A molecular basis for the differential roles of Bub1 and BubR1 in the spindle assembly checkpoint. *eLife* **4**, e05269. doi:10.7554/eLife.05269

Primorac, I., Weir, J. R., Chiroli, E., Gross, F., Hoffmann, I., van Gerwen, S., Ciliberto, A. and Musacchio, A. (2013). Bub3 reads phosphorylated MELT repeats to promote spindle assembly checkpoint signaling. *eLife* **2**, e01030. doi:10.7554/eLife.01030

Ricke, R. M. and van Deursen, J. M. (2013). Aneuploidy in health, disease, and aging. *J. Cell Biol.* **201**, 11-21. doi:10.1083/jcb.201301061

Rosenberg, J. S., Cross, F. R. and Funabiki, H. (2011). KNL1/Spc105 recruits PP1 to silence the spindle assembly checkpoint. *Curr. Biol.* **21**, 942-947. doi:10.1016/j.cub.2011.04.011

Santaguida, S. and Musacchio, A. (2009). The life and miracles of kinetochores. *EMBO J.* **28**, 2511-2531. doi:10.1038/emboj.2009.173

Saurin, A. T. (2018). Kinase and phosphatase cross-talk at the kinetochore. *Front. Cell Dev. Biol.* **6**, 62. doi:10.3389/fcell.2018.00062

Saurin, A. T., van der Waal, M. S., Medema, R. H., Lens, S. M. A. and Kops, G. J. P. L. (2011). Aurora B potentiates Mps1 activation to ensure rapid checkpoint establishment at the onset of mitosis. *Nat. Commun.* **2**, 316. doi:10.1038/ncomms1319

Silió, V., McAinsh, A. D. and Millar, J. B. (2015). KNL1-Bubs and RZZ provide two separable pathways for checkpoint activation at human kinetochores. *Dev. Cell* **35**, 600-613. doi:10.1016/j.devcel.2015.11.012

Skoufias, D. A., Andreassen, P. R., Lacroix, F. B., Wilson, L. and Margolis, R. L. (2001). Mammalian mad2 and bub1/bubR1 recognize distinct spindle-attachment and kinetochore-tension checkpoints. *Proc. Natl. Acad. Sci. USA* **98**, 4492-4497. doi:10.1073/pnas.081076898

Sliedrecht, T., Zhang, C., Shokat, K. M. and Kops, G. J. P. L. (2010). Chemical genetic inhibition of Mps1 in stable human cell lines reveals novel aspects of Mps1 function in mitosis. *PLoS ONE* **5**, e10251. doi:10.1371/journal.pone.0010251

Stukenberg, P. T. and Burke, D. J. (2015). Connecting the microtubule attachment status of each kinetochore to cell cycle arrest through the spindle assembly checkpoint. *Chromosoma* **124**, 463-480. doi:10.1007/s00412-015-0515-z

Sudakin, V., Chan, G. K. T. and Yen, T. J. (2001). Checkpoint inhibition of the APC/C in HeLa cells is mediated by a complex of BUBR1, BUB3, CDC20, and MAD2. *J. Cell Biol.* **154**, 925-936. doi:10.1083/jcb.200102093

Suzuki, A., Badger, B. L., Salmon, E. D., Kain, S. R. and Piston, D. W. (2015). A quantitative description of Ndc80 complex linkage to human kinetochores. *Nat. Commun.* **6**, 8161. doi:10.1038/ncomms9161

Tooley, J. and Stukenberg, P. T. (2011). The Ndc80 complex: integrating the kinetochore's many movements. *Chromosom. Res.* **19**, 377-391. doi:10.1007/s10577-010-9180-5

Vleugel, M., Tromer, E., Omerzu, M., Groenewold, V., Nijenhuis, W., Snel, B. and Kops, G. J. P. L. (2013). Arrayed BUB recruitment modules in the kinetochore scaffold KNL1 promote accurate chromosome segregation. *J. Cell Biol.* **203**, 943-955. doi:10.1083/jcb.201307016

Vleugel, M., Omerzu, M., Groenewold, V., Hadders, M. A., Lens, S. M. A. and Kops, G. J. P. L. (2015). Sequential multisite phospho-regulation of KNL1-BUB3 interfaces at mitotic kinetochores. *Mol. Cell* **57**, 824-835. doi:10.1016/j.molcel.2014.12.036

von Schubert, C., Cubizolles, F., Bracher, J. M., Sliedrecht, T., Kops, G. J. P. L. and Nigg, E. A. (2015). Plk1 and Mps1 cooperatively regulate the spindle assembly checkpoint in human cells. *Cell Rep.* **12**, 66-78. doi:10.1016/j.celrep.2015.06.007

Wei, R. R., Al-Bassam, J. and Harrison, S. C. (2007). The Ndc80/HEC1 complex is a contact point for kinetochore-microtubule attachment. *Nat. Struct. Mol. Biol.* **14**, 54-59. doi:10.1038/nsmb1186

Wendell, K. L., Wilson, L. and Jordan, M. A. (1993). Mitotic block in HeLa cells by vinblastine: ultrastructural changes in kinetochore-microtubule attachment and in centrosomes. *J. Cell Sci.* **104**, 261-274.

Wigge, P. A. and Kilmartin, J. V. (2001). The Ndc80p complex from Saccharomyces cerevisiae contains conserved centromere components and has a function in chromosome segregation. *J. Cell Biol.* **152**, 349-360. doi:10.1083/jcb.152.2.349

Zaytsev, A. V., Sundin, L. J. R., DeLuca, K. F., Grishchuk, E. L. and DeLuca, J. G. (2014). Accurate phosphoregulation of kinetochore-microtubule affinity requires unconstrained molecular interactions. *J. Cell Biol.* **206**, 45-59. doi:10.1083/jcb.201312107

Zaytsev, A. V., Mick, J. E., Maslennikov, E., Nikashin, B., DeLuca, J. G. and Grishchuk, E. L. (2015). Multisite phosphorylation of the NDC80 complex gradually tunes its microtubule-binding affinity. *Mol. Biol. Cell* **26**, 1829-1844. doi:10.1091/mbc.E14-11-1539

Zhang, G. and Nilsson, J. (2018). The closed form of Mad2 is bound to Mad1 and Cdc20 at unattached kinetochores. *Cell Cycle* **17**, 1087-1091. doi:10.1080/15384101.2018.1480209

Zhang, G., Lischetti, T. and Nilsson, J. (2014). A minimal number of MELT repeats supports all the functions of KNL1 in chromosome segregation. *J. Cell Sci.* **127**, 871-884. doi:10.1242/jcs.139725

Zhang, G., Mendez, B. L., Sedgwick, G. G. and Nilsson, J. (2016). Two functionally distinct kinetochore pools of BubR1 ensure accurate chromosome segregation. *Nat. Commun.* **7**, 12256. doi:10.1038/ncomms12256